Dynamic single-molecule force spectroscopy: bond rupture analysis with variable spacer length



2003 J. Phys.: Condens. Matter 15 S1709

(http://iopscience.iop.org/0953-8984/15/18/305)

INSTITUTE OF PHYSICS PUBLISHING JOURNAL OF PHYSICS: CONDENSED MATTER

J. Phys.: Condens. Matter **15** (2003) S1709–S1723 PII: S0953-8984(03)58905-6

# Dynamic single-molecule force spectroscopy: bond rupture analysis with variable spacer length

**Claudia Friedsam, Angelika K Wehle, Ferdinand Kühner and Hermann E Gaub**

Lehrstuhl für Angewandte Physik and Center for NanoScience, Ludwig-Maximilians-Universität München, Amalienstraße 58, 80799 München, Germany

Received 29 January 2003
Published 28 April 2003
Online at stacks.iop.org/JPhysCM/15/S1709

**Abstract**

Dynamic force spectroscopy is a valuable technique to explore the energy landscape of molecular interactions. Polymer spacers are typically used to couple the binding partners to the surfaces. To illustrate the impact of polymer spacers on the measured rupture force and loading rate distributions we used a Monte Carlo simulation, which was adjusted step by step towards realistic experimental conditions. We found that the introduction of a polymer spacer with a discrete length had only a marginal effect. However, a distribution of polymer spacers with different lengths may induce drastic changes on the distributions.

Three different methods for data analysis were then tested with regard to their ability to reproduce the input values of the Monte Carlo simulations. We found that simple linearization of all data points leads to an analysis error up to one order of magnitude for the dissociation rate and one-third for the potential width. The best results are achieved by determining the dissociation rate and the potential width directly with a probability density function for the rupture forces and the loading rates as a fit function that uses the dissociation rate and the potential width as fit parameters. By applying this method the analysis errors could be reduced below 25% for the dissociation rate and only 3% for the potential width.

Applied to a set of experimental data this method proved to be extremely useful and provided detailed information on the distributions. We are able to discriminate specific and non-specific contributions of an aptamer–ligand interaction and correct for the non-specific background. In addition, this procedure allowed us to account for the low force instrumentation cut-off and reconstruct the rupture force and force rate distributions.

(Some figures in this article are in colour only in the electronic version)

  

## 1. Introduction

Biomolecular bonds between large macromolecules result from an interplay of several weak interactions that combine to create a very stable aggregate. The constructs they form show in general long lifetimes and may withstand sizable mechanical loads.

Looking at one isolated bond which contributes to such an aggregate one may get a quite contrary impression: on timescales longer than its natural lifetime for spontaneous thermally driven dissociation, an isolated single bond has no strength and will dissociate under zero force. Consequently the lifetime of the bond may be shortened by external forces. This was first described by Bell [1] in 1978 who pointed out that bond failure is a statistical process and that the lifetime of a bond depends on the mechanical load. Bell's basic approach was refined by Evans *et al* in 1991 [2] and others who afterwards worked out a more extensive theory about the physics that underlies bond strength [3]. This theory was supported by numerous experimental results [4]. Dynamic force spectroscopy became a prominent method which provided new insight into the inner world of molecular interaction. Many of the common techniques make use of a polymer as spacer between the force sensor and the bond under investigation. The polymer can be regarded as an additional nonlinear spring. Thus—if the polymer is softer than the force sensor—the bond is subject to a non-steady loading rate. The effect of such a soft molecular linkage on the strength of a weak connecting bond has been examined in a theoretical way by Evans and Ritchie [5]. Building on the work of previous authors we used a Monte Carlo simulation to illustrate the impact of the polymer spacer on the distribution of the measured data points and to identify the optimal method for data analysis. The results of this study will give an overview about the relationship between the properties of the linkers and the distribution of the measured rupture forces. Step by step we provide a way to bridge the gap between measured and simulated data.

## 2. Theory

In most experiments bond dissociation occurs under dynamic load [6] and the theory has been worked out in great detail. Here we just want to present a shortened approach, which leads us to the central equations to which we will refer to in the course of this report.

The first theory concerning the reaction rate was developed by Arrhenius. Due to him the rate of dissociation $\lambda$ is given by the Van't Hoff–Arrhenius law [7]:

$$\lambda = \nu \exp\left(-\frac{\Delta G}{k_B T}\right). \tag{1}$$

Here $\nu$ is the natural vibration frequency of the bond in vacuum, $\Delta G$ is the free enthalpy, $k_B$ is the Boltzmann constant and $T$ is the temperature, respectively. For our applications we need a description of bond dissociation in liquids. Therefore we make use of the Kramers theory [8] and get an expression for the force dependent rate of dissociation in liquids:

$$\lambda(F) = \frac{\omega_{min}\omega_{max}}{2\pi\gamma} \exp\left(-\frac{(\Delta G - F\Delta x)}{k_B T}\right) = k^*_{off} \exp\left(\frac{F\Delta x}{k_B T}\right). \tag{2}$$

Here $\omega_{min}$ signifies the angular frequency of the metastable state, $\omega_{max}$ the positive valued angular frequency of the unstable state at the barrier, $\gamma$ the damping relaxation rate, $\Delta x$ the potential width and $k^*_{off}$ the natural off-rate.

The rate of dissociation can be used to describe the decline of the existing bonds $N_B$ with time,

$$\frac{\mathrm{d}N_B}{\mathrm{d}t} = -\lambda(t) N_B. \tag{3}$$

We obtain the number of intact bonds at time $t$ by integration of equation (2):

$$N_B(t) = \exp\left(-\int_0^t \mathrm{d}t'\,\lambda(t)\right). \tag{4}$$

According to this the number of dissociated bonds $N_D$ at time $t$ is given by

$$N_D(t) = 1 - N_B(t) = 1 - \exp\left(-\int_0^t \mathrm{d}t'\,\lambda(t)\right). \tag{5}$$

Assuming that the force is a reversible continuous function of time, time can be replaced by force, which results in the following expression:

$$N_D(t) = 1 - \exp\left(-\int_0^F \mathrm{d}f'\,\lambda(F)\frac{1}{\dot{f}}\right). \tag{6}$$

The probability $p(F)$ that the bond breaks if the force $F$ acts on it is given by $\frac{\mathrm{d}N_D}{\mathrm{d}F}$:

$$p(F) = \frac{\mathrm{d}N_D}{\mathrm{d}F}(F) = \lambda(F)\frac{1}{\dot{F}}\exp\left(-\int_0^F \lambda(F)\frac{1}{\dot{f}}\,\mathrm{d}f\right). \tag{7}$$

Equation (2) put into (7) leads to

$$p(F) = k^*_{off}\exp\left(\frac{F\Delta x}{k_BT}\right)\frac{1}{\dot{F}}\exp\left(-k^*_{off}\int_0^F \exp\left(\frac{F\Delta x}{k_BT}\right)\frac{1}{\dot{f}}\,\mathrm{d}f\right). \tag{8}$$

The maximum of this distribution points to the most probable rupture force $F^*$. It can be found by derivation:

$$\frac{\mathrm{d}}{\mathrm{d}F}\left(\frac{\mathrm{d}P_D}{\mathrm{d}F}(F)\right) = 0. \tag{9}$$

Assuming that the loading rate $\dot{F}$ is independent of the force $F$ we get a linear dependence of $F^*$ on the logarithm of the loading rate $\dot{F}$:

$$F^*(\dot{F}) = \frac{k_BT}{\Delta x}\ln\left(\frac{\dot{F}}{k^*_{off}}\frac{\Delta x}{k_BT}\right). \tag{10}$$

If we make use of a soft polymer spacer the loading rate which acts on the bond under investigation is changing continuously while the polymer is stretched. Therefore the condition that $\dot{F}$ is independent of $F$ is not fulfilled in our case and equation (10) is only an approximate description of our problem.

Equation (8) as well as equation (10) can be used to determine the natural off-rate $k^*_{off}$ and the potential width $\Delta x$ for a given distribution of rupture forces and corresponding loading rates. We will discuss this in detail below.

## 3. Monte Carlo simulations

In order to illustrate the influence of the polymer spacer and to generate a set of model data a Monte Carlo simulation was created and adjusted step by step to more realistic experimental conditions. The principle stays the same for all three types of Monte Carlo simulation: equation (2) is used to determine the probability for the bond rupture during the time slice $\Delta t$,

$$\Delta N_D = -\Delta N_B = -\lambda(t)\Delta t = -\lambda(F(t))\Delta t = k^*_{off}\exp\left(\frac{F\Delta x}{k_BT}\right)\Delta t. \tag{11}$$

This probability is compared to a random number between zero and unity. If the random number is smaller than $\Delta N_D$ the corresponding force is noted as the rupture force and the next iteration of the simulation is started. $k^*_{off}$ and $\Delta x$ are the two input values of the simulation. $F(t)$ determines the results.

### *3.1. Constant force rate*

In the simplest case we assume a linear dependence of the force on time. In the simulation this is realized by a force which increases linearly with the distance between the force sensor and the opposing surface which are separated with the velocity $v$. $F(t)$ is then given by

$$F(t) = \frac{\mathrm{d}F}{\mathrm{d}z} vt \qquad \text{with } \frac{\mathrm{d}F}{\mathrm{d}z} = \text{constant}, v = \text{constant}. \tag{12}$$

### *3.2. Polymer spacer*

In this simulation a polymer with a discrete length is introduced. The stretching of single polymers is well described by an extended Langevin function [9, 10]:

$$z(F) = L_1 N_M \left( \coth\left( \frac{F L_K}{k_B T} \right) - \frac{k_B T}{F L_K} \right) + N_M \frac{F}{K_M}. \tag{13}$$

Here $L_1$ represents the monomer length, $L_K$ the Kuhn length, $N_M$ the number of monomers and $K_M$ the monomer elasticity.

Certain polymers undergo conformational transitions upon stretching. As shown previously this can be modelled by a Markovian two-level system [11] and can be considered in the extension–force relation in the following way:

$$z(F) = N_M \left( \frac{L_2}{\mathrm{e}^{-\Delta G_{12}/k_B T} + 1} + \frac{L_1}{\mathrm{e}^{\Delta G_{12}/k_B T} + 1} \right) \left( \coth\left( \frac{F L_K}{k_B T} \right) - \frac{k_B T}{F L_K} \right) + N_M \frac{F}{K_M} + \frac{F}{k} \tag{14}$$

where $L_1$ signifies the monomer length in the initial conformation, $L_2$ the monomer length after the conformation transition and $\Delta G_{12}(F)$ the energy difference between the two states dependent on the applied force. For our calculations we additionally have to consider the deflection of the force sensor which is represented by the last term, where $k$ means the spring constant of the force sensor. We can use this relation to determine $F(t(z))$ and $\dot{F}(t(z)) = (\mathrm{d}F/\mathrm{d}z)^* v$ with $t(z) = z/v$. This type of simulation was used to demonstrate the influence of the elastic properties of the used polymer spacer on the distributions.

### *3.3. Gaussian and rectangular spacer lengths distributions*

Under realistic experimental conditions polymers show a length distribution which can be determined by fitting the experimental data. We have expanded the Monte Carlo simulation once again in such a way that it can operate on a given distribution of monomers. To realize this the simulation is done separately with every number of monomers that appears in the distribution. The number of iterations for every number of monomers is equal to its occurrence in the monomer distribution. Finally all data points are collected in a histogram. We let this simulation operate on a Gaussian length distribution and a rectangular length distribution.

## 4. Data analysis

Each simulation was performed ten times for ten different velocities of the force sensor, ranging from 100 to 1000 nm $\mathrm{s}^{-1}$ with steps of 100 nm $\mathrm{s}^{-1}$. This way we create ten different distributions of $(F^*, \ln(\dot{F}))$ data pairs for certain input values of $\Delta x$ and $k^*_{off}$. Altogether we create five sets of ten distributions for every type of simulation. These distributions were then analysed by three different methods. The resulting $k^*_{off}$ and $\Delta x$ of the different analysis methods were then validated by comparison with the initial values of the simulations.

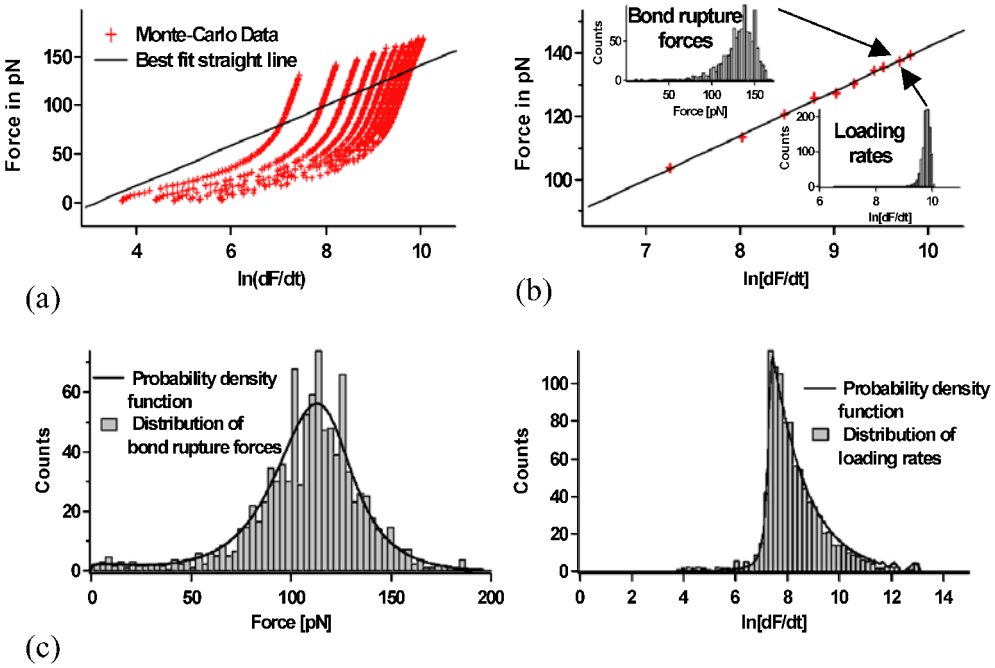


**Figure 1.** Illustration of the three methods described. (a) Method 1: diagram with all data points delivered by the polymer spacer simulation and best fit straight line. (b) Method 2: linearization of the most probable rupture forces and their loading rates. The maxima are determined in the histograms of the bond rupture forces and are plotted against the corresponding loading rates for the ten different velocities. The best fit straight line is determined for the ten resulting data pairs. (c) Method 3: one example for a histogram of the rupture forces and a histogram of the loading rates (logarithmic scale) for the rectangular length distribution simulation each overlaid with the best fit. The dissociation rate and the potential width are directly determined as fit parameters.

In *method 1* we just use all data pairs we obtained from the Monte Carlo simulation, plot them in a force over ln (loadingrate) diagram and determine the best fit straight line. The procedure is depicted in figure 1(a). On the basis of this line fit we can use equation (10) to determine $k^*_{off}$ and $\Delta x$,

$$\Delta x = \frac{k_B T}{m} \tag{15}$$

$$k^*_{off} = \frac{\dot{F}(F=0)\Delta x}{k_B T} \tag{16}$$

where $m$ signifies the slope of the best fit straight line.

*Method 2* determines the maxima of the rupture forces and the corresponding loading rates for each velocity and just plots these 10 points in the force over ln (loadingrate) diagram. The rest of the analysis is analogous to method 1.

*Method 3* (figure 1(c)) simply builds the mean value of the dissociation rates and the potential widths we obtained directly from the best fit curves which use these two sizes as fit parameters.

The fit curve is determined in the following way in each case.

For the linear force ramp we just use the constant loading rate $\dot{F}$ to calculate the pdf (pdf means probability density function) for the rupture force. The loading rate is discrete for every velocity in this case and therefore no separate fit is required.

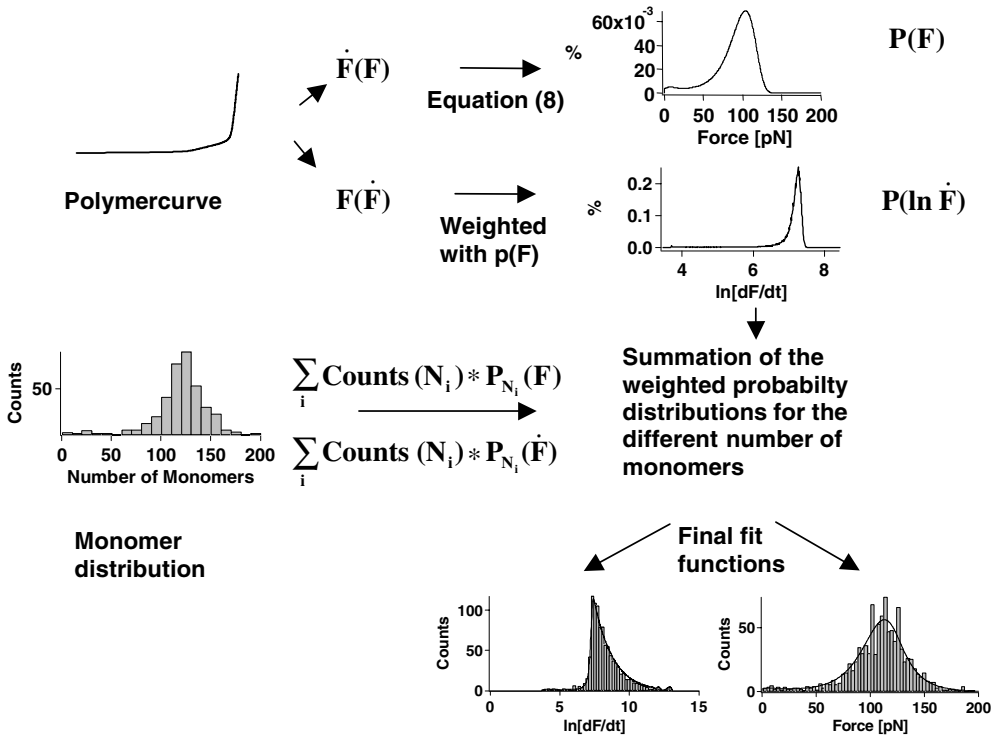


**Figure 2.** Construction of the pdfs. The upper part of the diagram illustrates how the pdfs for the bond rupture forces and their loading rates are determined in the case of a polymer spacer with a discrete length: each force is assigned to a loading rate by the polymer curve. Exploiting this relationship, the pdfs can be calculated. The pdf of the loading rates is just a 'translation' of the pdf for the rupture forces: each loading rate is assigned to a rupture force—again by the use of the polymer fit curve—and weighted with its proportion in the pdf of the forces. The lower part of the diagram shows how these single pdfs can be overlaid to form the fit function if the polymer spacers show a length distribution: the single pdfs have to be additionally weighted with the occurrence of their number of monomers $N_i$ in the number of monomers distribution. Finally, all single probability density functions are added to form the final fit function which is in a last step normalized.

In the case of the polymer spacer with discrete length every $F$ is assigned to the corresponding loading rate $\dot{F}$ which was determined using the fit curve (equation (15), figure 2(a)) for the polymer. This results in a function $\dot{F}(F)$ which can be used to determine the pdf for the rupture force. This pdf of the force was translated into the pdf of the loading rates by weighting the loading rate $\dot{F}(F)$ with the probability of the corresponding force $F$.

For the distribution of polymer spacers with different lengths (figure 2(b)) we calculated the pdf of the force for each spacer length separately, weighted this distribution with the occurrence of the spacer length in the length distribution and added all these curves to obtain the final fit function. To determine the fit function for the loading rate the pdf was again translated into a pdf of the loading rate for each spacer length the way we did it above. The pdfs were again weighted with the occurrence of the spacer length in the length distribution for the polymer spacers and added to obtain the final fit function.

## 5. Results for the model data

In figure 3 the probability densities for the rupture forces and the loading rates which result from the four different types of simulation are plotted. The pdf for the single polymer spacer is

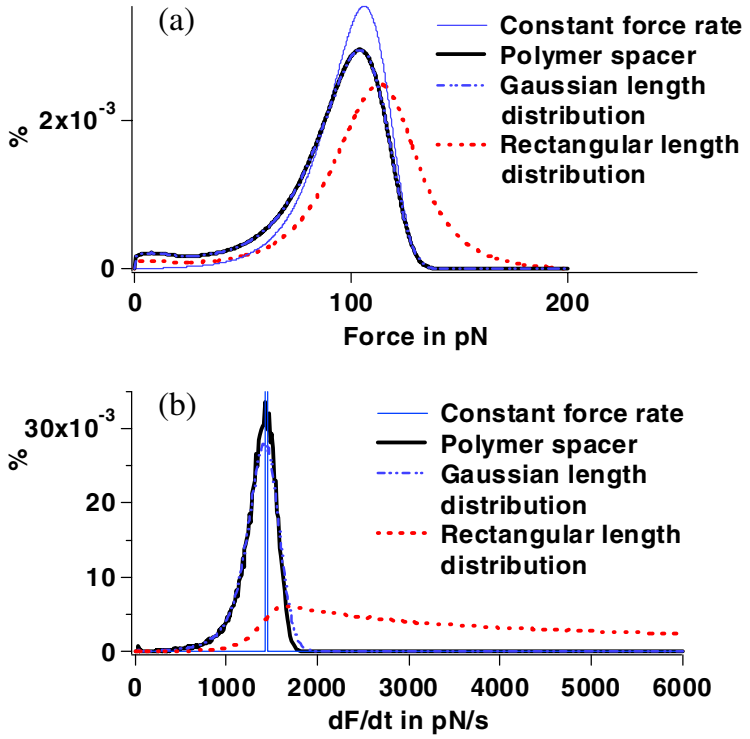


**Figure 3.** Pdfs of the rupture force and of the loading rate respectively for the four types of simulation. The input values were in all cases $k^*_{off} = 0.05\ \mathrm{s}^{-1}$ and $\Delta x = 3$ Å. The velocity of the force sensor was 100 nm $\mathrm{s}^{-1}$. The linear force ramp in the constant force rate simulation had a slope of 14 pN $\mathrm{nm}^{-1}$. The polymer in the polymer spacer simulation is represented by a polyethyleneglycol with $N_M = 150$ monomers and the following fit parameters [12]: $L_1 = 2.8$ Å, $L_2 = 3.58$ Å, $\Delta G_{12}(F) = 40$ eV, $L_K = 7$ Å, $K_M = 150\ \mathrm{N\ m}^{-1}$ and $k = 0.01\ \mathrm{mN\ m}^{-1}$. The Gaussian length distribution simulation works with a narrow Gaussian distribution for the number of monomers $N$ of the polymer spacer with $\bar{N} = 150$ and $\sigma_N = 10$ and the rectangular length distribution simulation is based on a rectangular distribution ranging from 1 to 150 monomers. (a) Pdfs of the rupture force. (b) Pdfs of the loading rates.

broadened compared to the one for the linear force ramp and the most probable rupture force is slightly shifted. The difference between the function for the single polymer spacer and the one for the Gaussian spacer length distribution is so small that it is not visible on this scale whereas the pdf for the rectangular distribution of polymer lengths differs significantly from the other ones: it is much broader and the most probable rupture force is shifted to higher values. The shape of the function is also different: it has completely lost the characteristics of an extreme value distribution. The obtained distribution is an overlay of many different extreme value distributions which results in the symmetric shape.

The linear force ramp results in a discrete loading rate for a given velocity of the force sensor. A polymer spacer with a discrete length results in a distribution of loading rates which is slightly broadened when a Gaussian length distribution is assumed for the polymer. In the case of the rectangular length distribution a very wide range of loading rates is obtained.

In figure 4 the rupture forces are plotted against the logarithm of the corresponding loading rate for each type of simulation. In the case of the linear force ramp (see figure 4(a)) the ten simulated velocities of the force sensor result in ten discrete loading rates. For each loading rate the forces show a distribution which follows the pdf of the rupture forces. When a polymer

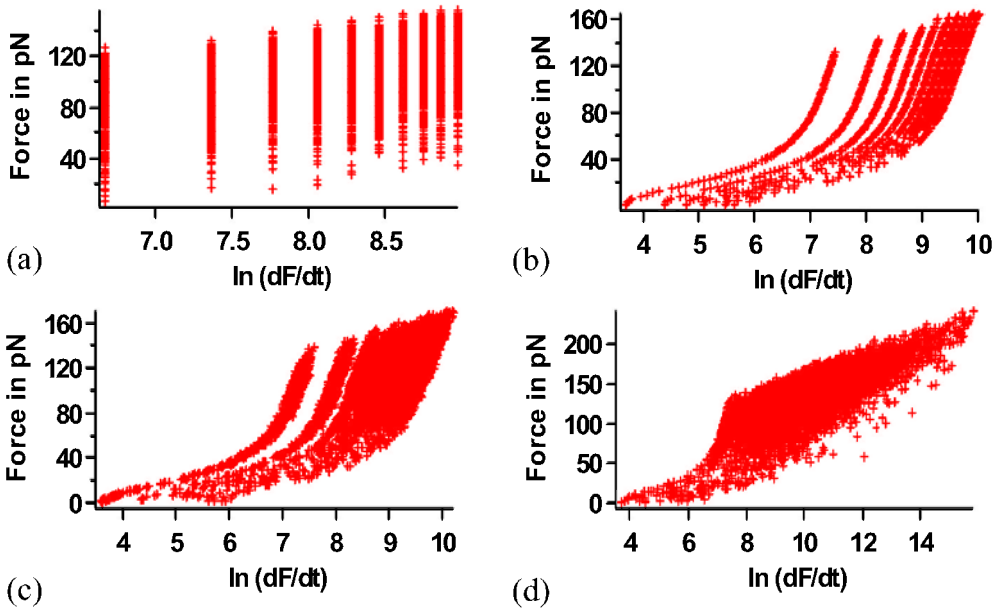


**Figure 4.** Distribution of the Monte Carlo data in an $F$ over $\ln(\dot{F})$ diagram for the four types of simulation. The input values were again $k^*_{off} = 0.05\ \mathrm{s}^{-1}$ and $\Delta x = 3$ Å. (a) Constant force rate simulation: the linear force ramp had a slope of 14 pN $\mathrm{nm}^{-1}$. (b) Polymer spacer simulation: the polymer was represented by a polyethyleneglycol with $N_M = 150$ monomers and fit parameters as in [12]. (c) Gaussian spacer length distribution simulation: the parameters of the Gaussian length distributions were $\bar{N} = 150$ and $\sigma_N = 10$. (d) Rectangular spacer length distribution simulation: the rectangular distribution ranged from one to 150 monomers.

spacer is introduced (see figures 4(b) and 3(a)) different rupture forces $F$ are correlated with different loading rates $\dot{F}(F)$. Thus for every velocity the data points lie on a curve which reflects the elastic properties of the polymer spacer. A narrow Gaussian distribution in length broadens these curves (see figure 4(c)). The rectangular length distribution results in 150 curves for each velocity. Altogether, a rather continuous distribution of $(F, \dot{F})$ data pairs for the ten velocities is obtained. Only on the edges of the whole distribution are the curves for 150 and one monomer(s) discernible.

In figure 5 the results for the three methods of data analysis are plotted. *Method 1* delivers satisfactory results only in the case of the linear force ramp: the potential width can be determined with a deviation of about $\pm 3\%$ but the values for the dissociation rates are all too high; they differ from the input value by a factor of about two. This can be explained in the following way: equation (10) is deduced from requirement (9). Therefore it is inevitable to use the most probable rupture forces and the corresponding loading rates for the ten simulated velocities to perform the linearization. In the case of the linear force ramp the linearization of all data points is equal to the linearization of the mean rupture forces of the ten given loading rates. As the mean rupture forces are slightly smaller than the most probable rupture forces the best fit straight line is shifted downwards and as a result the rate of dissociation determined with the help of equation (15) is too high. Applied to the polymer spacer simulation one ends up with a deviation of about one-third for the potential width and about one order of magnitude for the dissociation rate. The reason for this huge difference is that the possible data pairs $(F, \dot{F})$ for a certain velocity of the force sensor are determined by the polymer spacer and thus the possible rupture force for a given loading rate in general is neither identical with the

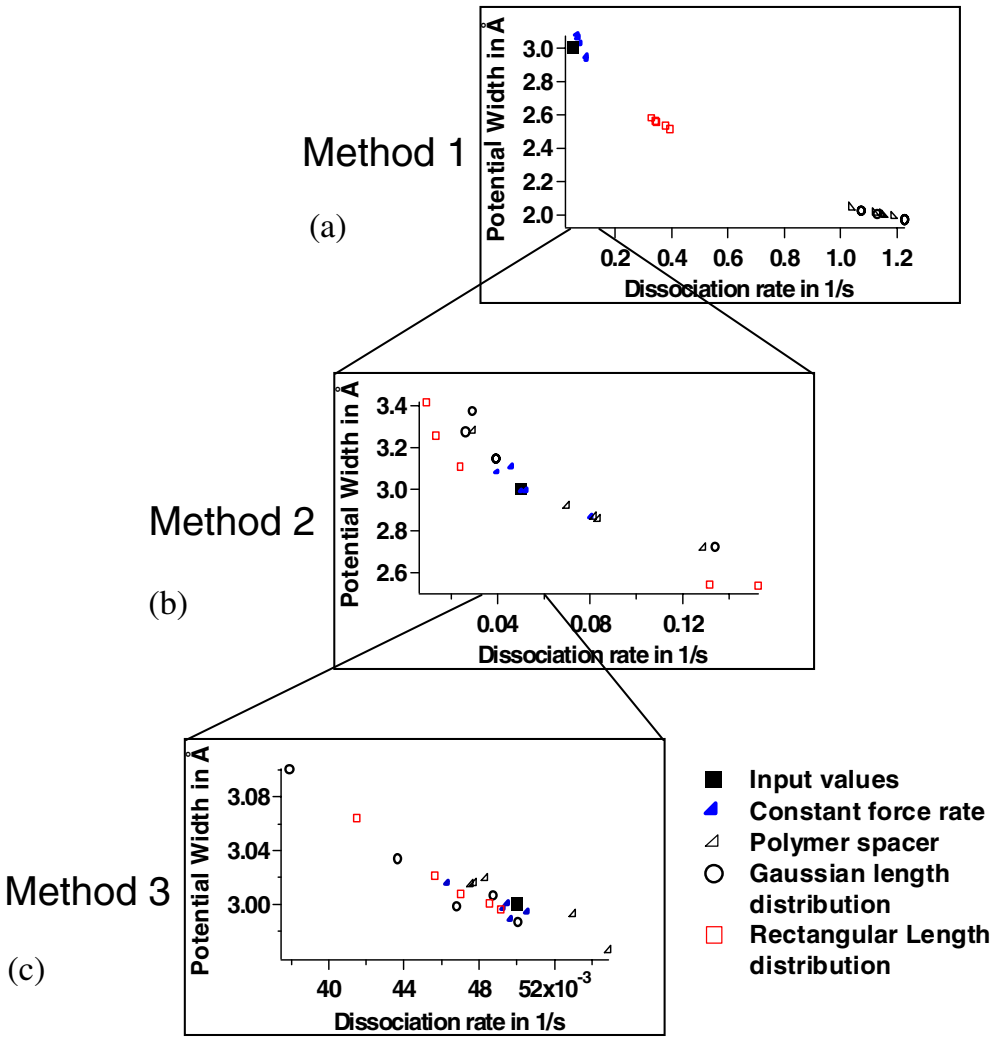


**Figure 5.** Results for the three tested methods of data analysis. Each of them is performed with the four different types of simulation illustrated in figure 4. In this succession of the methods the deviations from the input values from above decrease continuously. (a) Method 1: linearization of all data points. (b) Method 2: linearization of the maxima in the histograms. (c) Method 3: mean values of the determined fit parameters.

mean rupture force nor with the most probable rupture force, which belongs to the investigated bond for the given loading rate. The circumstances are more or less the same in the case of the Gaussian length distribution of the polymer spacer. On the other hand, the results get better for the rectangular length distribution. The deviation for the potential width is approximatively 15% and for the dissociation rate about a factor of eight. This is due to the fact that with the exception of the left-hand edge and the right-hand edge of the distribution of data points the system can adopt a variety of possible rupture forces for a given loading rate and therefore comes closer to the situation of the linear force ramp.

*Method 2*, which heeds the condition (9) and delivers values for $k^*_{off}$ and $\Delta x$, is the commonly used type of analysis for dynamic force spectroscopy. Applying this type of data analysis

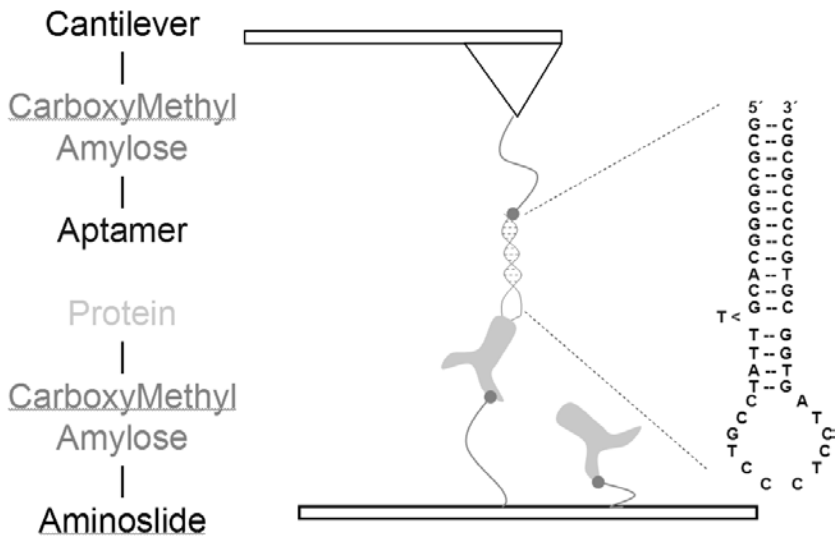


**Figure 6.** Set-up of the AFM experiment: the cantilever is aminosilanized and functionalized with carboxymethylamylose to which the aptamers are covalently bound in the side groups. The glass side is also aminofunctionalized and coated with carboxymethylamylose to which the human Ig-E is linked. The aptamers and the human Ig-E are allowed to form bonds during the experiment. As all other bonds are covalent and therefore much stronger the aptamer–Ig-E bond is ruptured when the cantilever is retracted.

one can obtain results that come relatively close to the input values for all four types of simulation (deviation for the potential width, at maximum 15%; deviation for the dissociation rate, at maximum a factor of two). The deviations for the dissociation rate can be easily explained if one remembers that equation (10) was derived under the condition that the loading rate $\dot{F}$ is independent from the rupture force $F$ which is questionable in our case where every loading rate $\dot{F}$ is attributed to one rupture force $F$ via the polymer curve. Therefore equation (10) just represents an approximation to our problem and it is quite natural that deviations appear.

On the other hand, *method 3* is only based on equation (8) which is an exact description of our problem. Due to this the results get better, the deviations are reduced to round 3% for the potential width and to round 25% for the dissociation rate, respectively. As a final conclusion it should be noted that this method represents the best approach to analyse experimental data in a sensible way.

## 6. Transfer to the experiment

In order to test the feasibility of our method with experimental data, we analysed a series of AFM measurements, which investigated the affinity of aptamers to human Ig-E antibodies.

Aptamers [13] are small, *in vitro* selectable single-stranded nucleic acids that are capable of binding proteins and other molecules with specificity and dissociation constants similar to those of antibodies. The aptamer D17.4ext (ext is the abbreviation for an extended D17.4 [14]) has a length of 45 nucleic acids and forms a stem–loop structure, which has a dissociation constant ($K_d$) of about 3.6 nM for human Ig-E [15]. The cantilever was functionalized with the aptamer via polymerspacers—in our case carboxymethylamylose—to avoid nonspecific binding. The human Ig-E was immobilized in the same way on the substrate. The set-up is shown in figure 6. One example for measured bond rupture histograms and their corresponding loading rates is shown in figure 7.

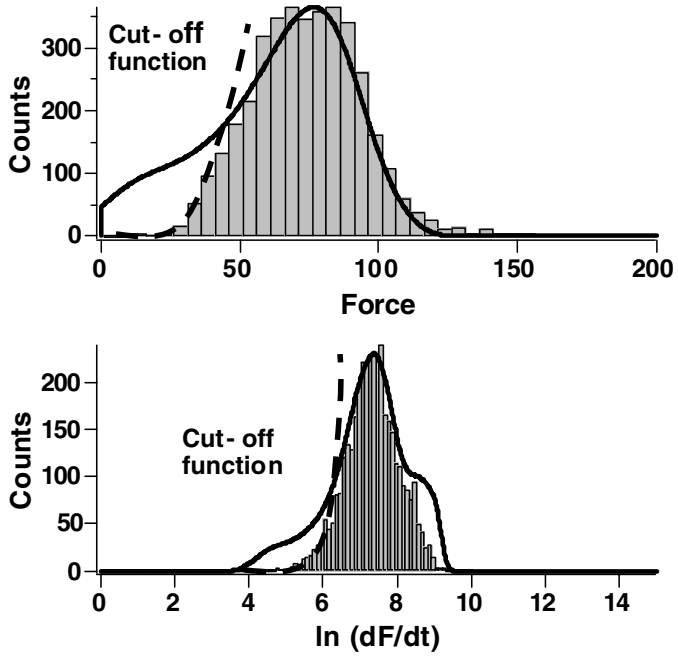


**Figure 7.** Example for an experimentally determined force distribution and the according loading rate distribution that can be fitted well with the developed algorithm. The fit parameters were $k^*_{off} = 3.3\ \mathrm{s}^{-1}$ and $\Delta x = 0.22$ Å. The dashed curve represents a schematic drawing of the cut-off function of our instrument.

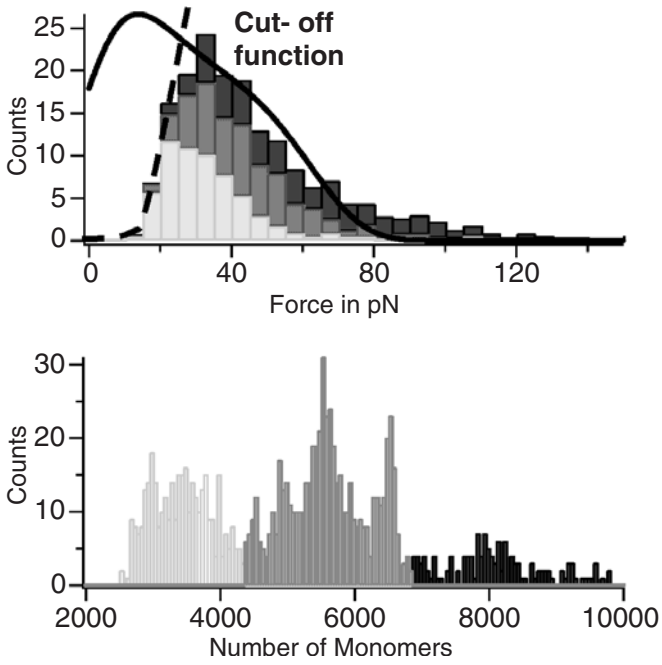


**Figure 8.** This diagram shows how different spacer length regimes contribute to the whole distributions which are fitted with $k^*_{off} = 3.3\ \mathrm{s}^{-1}$ and $\Delta x = 0.22$ Å as fit parameters. The dashed curve represents a schematic drawing of the cut-off function of our instrument.

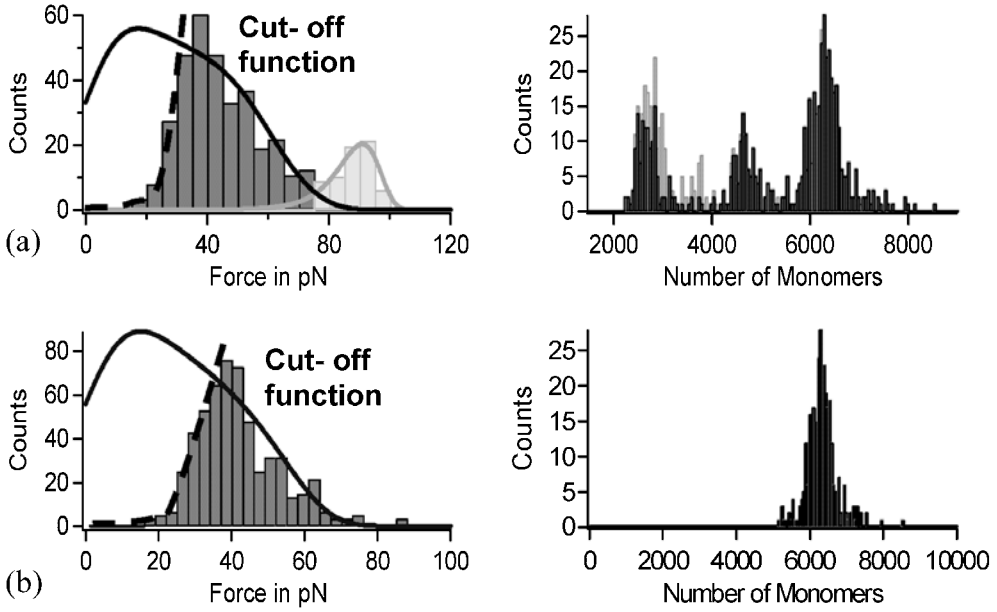


**Figure 9.** (a) Example where the identification of non-specific contributions was possible: histogram of the rupture forces, histogram of the loading rates and histogram of the number of monomers of the polymer spacer (which reflects the rupture length distribution). It is not possible to fit the force histogram and the loading rate histogram as a whole, if the calculation is based on the whole monomer distribution. Instead the distributions can be fitted with two different fit function with $k^*_{off} = 0.22\ \mathrm{s}^{-1}$ and $\Delta x = 3.5$ Å for the lower force regime and $k^*_{off} = 2.5 \times 10^{-5}\ \mathrm{s}^{-1}$ and $\Delta x = 7$ Å for the higher force regime, respectively. (b) Histograms of the rupture forces and histogram of the loading rates with an overlaid fit, for the case where just the part of the monomer distribution shown on the right is taken into consideration. The distributions can be fitted as a whole with $k^*_{off} = 0.22\ \mathrm{s}^{-1}$ and $\Delta x = 3.5$ Å.

We found that most of the distributions for the rupture forces and their loading rates can be fitted consistently by the developed fit functions (method 3) and deliver values for the dissociation rates between 0.17 and 0.3 $\mathrm{s}^{-1}$ and for the potential widths between 2.8 and 3.5 Å, respectively.

If the spacer length distribution shows discrete peaks different length regimes can easily be attributed to different bond rupture force and loading rate regimes. Figure 8 shows how these different contributions overlay to form the overall distributions which can be fitted with a potential width of 3.3 Å and a dissociation rate of 0.22 $\mathrm{s}^{-1}$.

In some cases it was not possible to fit the distribution of rupture forces and the distribution of loading rates with the same set of fit parameters. By separately analysing the bond rupture events which belong to the third peak in the polymer length distribution, we obtain the histograms shown in figure 9(b). The best fit of the distributions results in a potential width of 3.5 Å and a dissociation rate of 0.22 $\mathrm{s}^{-1}$ which is well comparable to the values obtained before. In turn by analizing the second peak in the bond rupture histogram of figure 9(a) separately we obtain values of 7 Å and $2.5 \times 10^{-5}\ \mathrm{s}^{-1}$ for the potential width and the dissociation rate, respectively, which could be explained by a non-specific adsorption of the protein. This procedure allows to separate different classes of events by analizing the populations in the histograms individually.

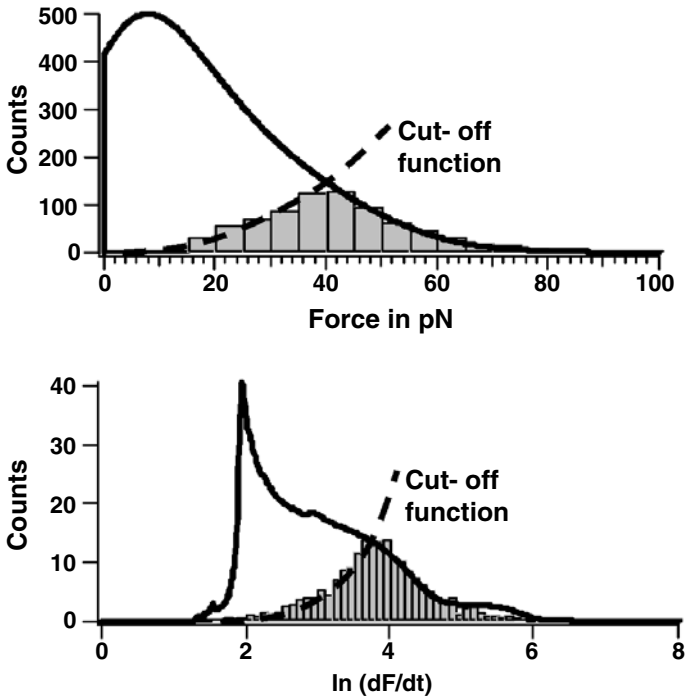


**Figure 10.** Example for an experiment where the dominant part of the distributions was not recorded because of the instrumental resolution limit: if we rely only on events with rupture forces over 40 pN the distributions are fitted with $k^*_{off} = 0.2\ s^{-1}$ and $\Delta x = 2.9$ Å as fit parameters. The dashed curve again represents a schematic drawing of the cut-off function of our instrument.

In figure 10 the distributions obtained for a very low velocity are depicted. The attempt to fit both distributions of rupture forces and loading rates simultaneously fails. Since a conservative estimate of the signal to noise ratio of our instrument lowers the force resolution to 40 pN, only higher rupture forces in the histogram in figure 10 were used for further analysis. With this limitation the distributions can be fitted with values of 2.9 Å for the potential width and $0.2\ s^{-1}$ for the dissociation rate. These values correspond well with the ones we obtained from other experiments. At least partially, this method also allows us to analyse nearly truncated histograms in a meaningful way.

## 7. Conclusions

Following the course of the four different Monte Carlo simulations one gets an impression of the changes in the distributions if the simulation is adjusted step by step to more realistic experimental conditions. The introduction of the polymer spacer leads to a distribution of the loading rates and induces a variation in the force distribution. Dependent on its shape a length distribution of the polymer spacer may alter the results for the rupture forces noticeably. Thus for some cases it is essentially necessary to implement the experimentally determined length distribution in the simulation in order to obtain data that are comparable to the experimental results.

We used the distributions produced by the Monte Carlo simulations as model data in order to identify the best among three tested methods for data analysis. Simple linearization of all data points is a systematically wrong method and in most cases leads to obviously

wrong results. Hence this method cannot be recommended for any of the simulated situations. Alternatively rather good results are obtained if the most probable rupture forces and their loading rates for the different velocities are linearized. But it is most favourable to determine the rate of dissociation and the potential width directly as fit parameters when we approximate the distribution of the rupture forces with a fit-function that is based on equation (8).

The application of this method to experimental data leads to very convincing results and reveals detailed information. We found in a certain number of experiments a very clear fit of the histograms to one set of potential width and dissociation rate values. In other experiments there was an overlay with non-specific interactions, but they could be separated by separately treating certain peaks in the number of monomers distribution of the polymer spacer. In other cases these non-specific signals overwhelm the specific contribution and no meaningful fit to these histograms was possible. Anyway, this may be due to the multiplicity of possible non-specific interactions, which, if they dominate the histograms, cannot be separated any more.

From the practical point of use the reconstruction of the histogram in the 'blind spot' of the instrument seems most attractive and has in our hands helped to markedly relativize the interpretation of data in the low force regime.

## Acknowledgments

Helpful discussions with Helmut Grubmüller and Daniel Güttler are thankful acknowledged. This work was supported by BMBF.

## References

[1] Bell G I 1978 *Science* **200** 618–27
[2] Evans E, Berk D and Leung A 1991 *Biophys. J.* **59** 838–48
[3] Evans E and Ritchie K 1997 *Biophys. J.* **72** 1541–55
Israilev S, Stepaniants S, Balsera M, Ono Y and Schulten K 1997 *Biophys. J.* **72** 1568–81
Grubmüller H, Heymann B and Tavan P 1996 *Science* **271** 997–9
[4] Rief M, Oesterhelt F, Heymann B and Gaub H E 1997 *Science* **275** 1295–7
Grandbois M, Beyer M, Rief M, Clausen-Schaumann H and Gaub H E 1999 *Science* **283** 1727–30
Rief M, Pascual J, Saraste M and Gaub H E 1999 *J. Mol. Biol.* **286** 553–61
Merkel R, Nassoy P, Leung A, Ritchie K and Evans E 1999 *Nature* **397** 50–3
Strunz T, Oroszlan K, Shafer R and Gutherodt H-J 1999 *Proc. Natl Acad. Sci. USA* **96** 11277–82
Dammer U, Hegner M, Anselmetti D, Wagner P, Dreier M, Huber W and Güntherodt H-J 1996 *Biophys. J.* **70** 2437–41
Dettmann W, Grandbois M, André S, Benoit M, Wehle A, Kaltner H, Gabius H-J and Gaub H E 2000 *Arch. Biochem. Biophys.* **383** 157–70
Evans E and Ludwig F 2000 *Phys. Condens. Matter* A **12** 315–20
Krüger D, Fuchs H, Rousseau R, Marx D and Parrinello M 2002 *Phys. Rev. Lett.* **89** 186402–(1–4)
Allemand J-F, Bensimon D, Jullien L, Bensimon A and Croquette V *Biophys. J.* **73** 2064–70
Thomson N H, Fritz M, Radmacher M, Schmidt C F and Hansma P K 1996 *Biophys. J.* **70** 2421–31
[5] Evans E and Ritchie K 1999 *Biophys. J.* **76** 2439–47
[6] Evans E 2001 *Annu. Rev. Biomol. Struct.* **30** 105–28
Evans E 1999 *Biophys. Chem.* **82** 83–97
Evans E 1998 *Faraday Discuss.* **111** 1–16
Heymann B and Grubmüller H 2000 *Phys. Rev. Lett.* **84** 6126–9
Heymann B and Grubmüller H 2001 *Biophys. J.* **81** 1295–313
Heymann B and Grubmüller H 1999 *Chem. Phys. Lett.* **303** 1–9
Balsera M, Stepaniants S, Israilev S, Oono Y and Schulten K J 1997 *Biophys. J.* **73** 1281–7
Boresch S and Karplus M 1995 *J. Mol. Biol.* **254** 801
Shillcock J and Seifert U 1998 *Phys. Rev.* E **57** 7301–4
Seifert U 2000 *Phys. Rev. Lett.* **84** 2750–3

[7] Arrhenius S 1889 *Z. Phys. Chem. Lpz.* **4** 226
Van't Hoff J H 1884 *Etudes de Dynamiques Chimiques* (Amsterdam: Muller) p 114
[8] Kramers H A 1940 *Physica (Utrecht)* **7** 284
Hänggi P, Talkner P and Borkovec M 1990 *Rev. Mod. Phys.* **62**
[9] Rief M, Gautel M, Oesterhelt F, Fernandez J M and Gaub H E 1997 *Science* **275** 1295–8
Smith S B, Cui Y and Bustamante C 1996 *Science* **271** 795–8
[10] In the meantime there are alternative polymer models:
Livadaru L, Netz R R and Kreuzer H J 2003 *J. Chem. Phys.* **118** 1404
Netz R R and Andelman D 2002 *Encyclopedia of Electrochemistry* ed M Urbakh and E Giladi (New York: Wiley–VCH)
Fleck C, Netz R R and von Grünberg H H 2002 *Biophys. J.* **82** 76
[11] Cluzel P, Lebrun A, Heller C, Lavery R, Vivoy J-L, Chateny D and Caron F 1996 *Science* **271** 792–4
Rief M, Fernandez J M and Gaub H E 1998 *Phys. Rev. Lett.* **81** 4764–7
[12] Oesterhelt F, Rief M and Gaub H E 1999 *New J. Phys.* **1** 6.1–6.11
Tadokoro H 1990 *Structure of Crystalline Polymers* (Malabar, FL: Krieger)
[13] James W 2000 *Encyclopedia of Analytical Chemistry* ed R A Meyers pp 4848–71
[14] Wiegand T W, Williams P B and Dreskin S C 1996 *J. Immunol.* **157** 221–30
[15] Liss M, Petersen B, Wolf H and Prohaska E 2002 *Anal. Chem.* **74** 4488–95